AGU ADVANCING EARTH AND SPACE SCIENCES

Space Weather

RESEARCH ARTICLE
10.1029/2025SW004753

Collection, Collation, and Comparison of Near-Earth In Situ CME Boundaries

C. Kay[1], E. E. Davies[2], M. Dumbović[3], K. Martinić[3], E. Palmerio[4], H. T. Rüdisser[2,5], E. Weiler[2,5], and C. Möstl[2]

[1]The Johns Hopkins University Applied Physics Laboratory, Laurel, MD, USA, [2]Austrian Space Weather Office, GeoSphere Austria, Graz, Austria, [3]Faculty of Geodesy, University of Zagreb, Hvar Observatory, Zagreb, Croatia, [4]Predictive Science Inc., San Diego, CA, USA, [5]Institute of Physics, University of Graz, Graz, Austria

Key Points:

- We combine existing near-Earth in situ CME boundary catalogs into a meta-catalog (1996–2006) and provide a new set of boundaries with mixed regions
- We compare sheath/flux rope properties derived using different catalogs and find small but statistically significant variations
- Different boundaries influence flux rope orientation reconstructions and cause variations of order 10° in latitude and 40° in longitude

Supporting Information:

Supporting Information may be found in the online version of this article.

Correspondence to:

C. Kay,
christina.kay@jhuapl.edu

Citation:

Kay, C., Davies, E. E., Dumbović, M., Martinić, K., Palmerio, E., Rüdisser, H. T., et al. (2026). Collection, collation, and comparison of near-Earth in situ CME boundaries. *Space Weather*, *24*, e2025SW004753. https://doi.org/10.1029/2025SW004753

Received 6 OCT 2025
Accepted 10 MAR 2026

Author Contributions:

Conceptualization: C. Kay
Data curation: C. Kay
Formal analysis: E. E. Davies, M. Dumbović, K. Martinić, E. Palmerio, H. T. Rüdisser, E. Weiler, C. Möstl
Investigation: C. Kay
Methodology: C. Kay
Software: C. Kay
Visualization: C. Kay
Writing – original draft: C. Kay
Writing – review & editing: E. E. Davies, M. Dumbović, K. Martinić, E. Palmerio, H. T. Rüdisser, E. Weiler, C. Möstl

Abstract Coronal mass ejections (CMEs) drive space weather throughout the heliosphere so knowledge of their internal properties is key to understanding and eventually forecasting their effects. Typically observations are limited to single-spacecraft encounters sampling one path that may or may not be representative of the overall structure. Many catalogs exist listing the observed boundaries of a CME ejecta and any CME-driven sheath. Often there are large differences in the reported boundaries across different catalogs. We introduce the Living List of Attributes Measured in Any In situ CME Encounter (LLAMAICE), which collects and collates existing near-Earth catalogs into a new meta-catalog. We have added a new set of boundaries, building upon the existing information that includes additional mixed regions containing mixed signatures of the pristine sheath and ejecta core (EC). This first version of LLAMAICE covers February 1995 to December 2006, corresponding to 1,516 entries for 396 unique CMEs. We use LLAMAICE to quantify the variation in mean sheath/ejecta properties from using boundaries from different catalogs and/or data from using ACE versus Wind data. We also reconstruct flux rope (FR) orientation for each set of bounds/spacecraft, which are well-known to be quite sensitive. For both studies, the cross-catalog variations exceed the cross-spacecraft variations. The reconstructed FR handedness agrees 77% of the time between spacecraft but only 47% across catalogs. The orientations vary between spacecraft by 2.2°/3.4° in inclination/longitude but 4/10 times that between catalogs.

Plain Language Summary Coronal mass ejections (CMEs) are large eruptions in the solar atmosphere that travel out into the solar system. When they hit a spacecraft we can measure their internal properties, like magnetic field, velocity, temperature, and density, which are important to understanding their space weather effects. Many catalogs exist listing the observed boundaries of CMEs, but quite often they do not agree with one another. Understanding these events is hard because it is difficult to interpret what a spacecraft observes during a single pass through such a large, complicated object. We have made a new catalog combining the results of existing catalogs, facilitating comparison of all the existing information. We add our own set of boundaries that builds upon the existing catalogs but allows for uncertain regions with a mixture of signatures. We use this meta-catalog to understand how sensitive derived results are to the chosen CME boundaries. First, we look at how the average CME properties vary across different catalogs. Second, we use a common method to reconstruct the CME orientation from the observations. This technique is known to be sensitive to the boundaries and we are able to better quantify the uncertainty in the reconstruction.

1. Introduction

Coronal mass ejections (CMEs), large explosions of material propagating outward from the Sun, drive the most significant space weather effects at Earth and throughout the solar system. Understanding the physics behind their eruption and evolution is important for fundamental physics research and predicting their effects is critical for space weather predictions. Building this knowledge depends on interpreting projected remote images combined with limited single-pass in situ spacecraft observations, and often accounting for an observational gap between the two. Given these limitations, researchers often do not reach a consensus on the interpretation of the in situ signatures of a CME and any CME-driven shock.

While singular, historical events have recorded CME observations as early as the 1860s (e.g., Eddy, 1974), consistent scientific observations began a century later. The Interplanetary Monitoring Platform (IMP) series of spacecraft, launched between 1963 and 1973, provided some of the earliest continuous near-Earth in situ observations. These in situ observations not only provided insights into the continuous solar wind (SW) but also the

transient CME events. More recently the Wind (Ogilvie & Desch, 1997) and Advanced Composition Explorer (ACE; Stone et al., 1998) spacecraft, both at the first Lagrange point (L1) roughly 0.01 au upstream of Earth, have provided three decades of largely-continuous in situ measurements. The launch of the twin Solar Terrestrial Relations Observatory (STEREO; Kaiser et al., 2008) provided an opportunity for near-1 au in situ measurements at longitudes away from the Earth, but also potential simultaneous measurements of the same CME from spatially separated spacecraft (e.g., Lugaz et al., 2024; Mulligan et al., 2013).

The earliest semi-routine remote observations of CMEs in the white-light corona started in the 1970s with the Orbiting Solar Observatory 7 (OSO-7) and Skylab, slightly later than the routine in situ measurements. Similar in timing to ACE and Wind for in situ observations, the Solar and Heliospheric Observatory (SOHO; Domingo et al., 1995) began routine observations in 1995 and has been a critical asset for remote CME observations ever since. The STEREO spacecraft presented an opportunity for multiple remote perspectives of the same event (e.g., Colaninno & Vourlidas, 2015), allowing for the development of numerous stereoscopic reconstruction techniques (e.g., Millward et al., 2013; Thernisien et al., 2009).

Continuous remote and in situ observations enabled a better understanding between the white light CME structures and their interplanetary counterparts. A simplified picture developed with the bright leading edge and dark cavity seen in white light remote images corresponding to a pile up of coronal plasma and the magnetically-dominated erupting flux rope (FR), which matches the density enhancement and magnetic structure often seen in in situ measurements (Schwenn, 2006, and references within). In some instances a shock can be observed ahead of the bright leading edge of the CME (e.g., Vourlidas et al., 2003) and the corresponding shock signatures are not uncommon in 1 au observations.

While this simplified picture is a useful model for the general physical processes at play, many additional effects take place during a CME's propagation that can alter the resulting in situ profiles. CMEs can deform or pancake (e.g., Davies et al., 2021; Savani et al., 2011), deflect (e.g., Kay et al., 2015; Wang et al., 2004), and erode (e.g., Dasso et al., 2007; Ruffenach et al., 2015) in addition to interacting with other CMEs (e.g., Lugaz et al., 2017; Scolini et al., 2020) or high speed streams (HSSs) (e.g., Palmerio et al., 2022; Webb & Howard, 2012). In situ CME catalogs often classify events based on how well their profiles fit an idealized structure. In particular, L. Burlaga et al. (1981) and Klein and Burlaga (1982) defined a magnetic cloud (MC) as a region with properties representative of the idealized structure of a magnetic FR. This includes an enhanced magnetic field strength (B), smooth rotation in the B vector, linearly decreasing plasma speed profile, as well as a decrease in temperature (T) and plasma beta (β). Other common signatures include bidirectional electrons (BDEs; Gosling et al., 1990) and composition/charge state variations (e.g., Aguilar-Rodriguez et al., 2006; Lynch et al., 2003). For further information on in situ CME signatures see reviews by Zurbuchen and Richardson (2006) and Kilpua et al. (2017).

Often observations do not include an idealized MC so various terms are used to refer to the FR-like magnetic portion, which is typically separated from the sheath of piled-up material preceding it. These terms include magnetic obstacle, (complex) ejecta, shock driver, piston, and magnetic blob. The term interplanetary CME (ICME) is also used, but sometimes this definition also includes the sheath region. One must be cautious when comparing across different catalogs to match different terminology for the same region. In this paper we will refer to this region as the ejecta core (EC) for simplicity, regardless of whether the in situ signatures exhibit all, some, or barely any of the expected idealized MC/FR behavior.

Many theoretical models exist to produce the enhanced, smoothly rotating magnetic signatures of an idealized FR. While the precise equations differ between models, they are all constrained by a set of parameters defining the orientation and FR properties. For observed events, one can combine the in situ profile with minimization techniques to infer the optimal input parameters (Hu & Sonnerup, 2002; Lepping et al., 1990; Sonnerup & Cahill, 1967). This methodology has been extensively used to reconstruct the in situ orientation of observed events and compare to the orientation expected from remote images (Al-Haddad et al., 2013; Möstl et al., 2009). Quite often these two orientations are not in agreement, suggesting either significant interplanetary evolution or large uncertainties in at least one of the reconstructions (Al-Haddad et al., 2018; Palmerio et al., 2018). This may be partially due to the expectation for real-world CMEs to match oversimplified global-scale cartoons when they likely exhibit significant local variations (Al-Haddad & Lugaz, 2025; Owens et al., 2017), where even small longitudinal separations between spacecraft have been found to result in significantly different event observations and properties (e.g., Davies et al., 2020; Palmerio et al., 2024; Regnault et al., 2024). However, in situ

reconstructions have also been found to vary significantly for small changes in the precise boundaries used for reconstructions (Al-Haddad et al., 2019; Lynch et al., 2022; Riley et al., 2004). Further analysis is needed to determine the extent to which single-pass in situ reconstructions can be used to describe the large-scale configuration of CMEs.

A large number of catalogs exist for both remote CME reconstructions and CME boundaries from in situ observations. Kay and Palmerio (2024) established the Living List of Attributes Measured in Any Coronal Reconstruction (LLAMACoRe), combining remote CME catalogs into a single meta-catalog with entries collated for each real-world event. LLAMACoRe was meant to be the first component of a larger LLAMAVERSE (Living List of Attributes Measured in Any Verified External Resource for Solar Events), a repository where all the existing but isolated data sets can be combined.

This work further builds the LLAMAVERSE with the Living List of Attributes Measured in Any In situ CME Encounter (LLAMAICE) using the existing catalogs of in situ CME boundaries near 1 au. In this work, we focus on near-Earth CME detections by Wind and ACE over the range 1996–2006—that is, approximately from the launch of Wind until the launch of STEREO. Ultimately we intend for it to include all events observed near-Earth, but begin with this first set and will expand it in future work. In Section 2 we describe the individual source catalogs used to build LLAMAICE, how we combined them and created a new set of boundaries, and provide a general overview of the results. Sections 3 and 4 use LLAMAICE to illustrate how sensitive average CME properties and reconstructed orientations are to the chosen boundaries and spacecraft.

2. LLAMAICE

We set to compile all the existing near-Earth in situ CME boundary catalogs into a single meta-catalog. We first introduce the source catalogs before discussing the collation of events and LLAMAICE boundaries. We note that we have both a LLAMAICE catalog and LLAMAICE boundaries. The catalog refers to the collated collection of all the existing catalog boundaries. The boundaries refer to a new set of boundaries generated by this team based upon the existing catalog information as well as the in situ observations themselves.

2.1. Individual Source Catalogs

We list the existing sources used to build the LLAMAICE catalog. The text in bold represents the shorthand name we will use for that catalog throughout this work, followed by a brief description of the boundaries each catalog includes and any criteria provided by the authors for selecting those boundaries.

1. *CDAW*—The Coordinated Data Analysis Group (CDAW) held a series of meetings, including one dedicated to FR observations. They established a catalog of boundaries of shock-driving CMEs from solar cycle 23, selecting from the events within Gopalswamy et al. (2010) those with source region within 15° of the central meridian (as seen from Earth). They report a shock time and an "ICME" start and end. The ICME boundaries are set to the region of "proton temperature depression" following the shock. The list can be found at https://cdaw.gsfc.nasa.gov/meetings/2010_fluxrope/LWS_CDAW2010_ICMEtbl.html
2. *DREAMS* (Chi et al., 2016)—The Data REseArch and More in Space physics (DREAMS) catalog includes in situ events observed by Wind during 1995–2015. Each entry includes a shock time (when appropriate) and an "ejecta" start and end. They consider six different criteria (enhanced B, smoothing rotating B components, declining solar wind speed profile, low proton T, low plasma β, and BDEs). Events are classified as an ICME if three or more criteria are satisfied. The catalog can be found at https://space.ustc.edu.cn/dreams/wind_icmes/index.php.
3. *Jian* (Jian et al., 2006)—This catalog collects events between 1995 and 2004 and reports an event start and the start and end of a "magnetic obstacle" (MO). The event start corresponds to the "outer distinct plasma and magnetic field discontinuities" and will correspond to either a shock, a pile up in front of the ejecta, or potentially the ejecta itself if there is no sheath. We assume the presence of a sheath when the event start occurs before the MO start. Both Wind and ACE measurements are considered but boundaries are reported using the Wind timing whenever possible. Jian et al. (2006) visually identify events using the "total perpendicular pressure" as well more traditional plasma signatures (low proton T, enhanced B, smooth B component rotation, enhanced helium abundance, BDEs).
4. *Lepping* (Lepping et al., 2006, 2020)—This catalog represents a set of papers identifying MCs in Wind observations and fitting their profiles with a static, force free, cylindrically-symmetric, Lundquist FR model. The

catalog does not include a shock time. The primary factors in determining the flux rope boundaries are the proton β, proton T, average speed and speed profile, B intensity and orientation, and in some cases the results of the FR fitting procedure.

5. *RC* (Richardson & Cane, 2010, 2024)—This catalog is a regularly-updated list of CMEs primarily observed by ACE but also referring to IMP8, Wind and OMNI as needed during data gaps. It includes a "disturbance" time and an "ICME" start and stop time. The disturbance time corresponds to the onset of geomagnetic storm commencement, often corresponding to the CME-driven shock impacting the Earth, which will occur shortly after it passes ACE at L1. The ICME times are rounded to the nearest hour. This catalog includes columns for MC start and stop times as taken from either Huttunen et al. (2005) or the Lepping catalog. Only a small portion of the RC entries include MC values, and many of these are duplicates of the Lepping list so we do not use these MC times in this study. We infer the presence of a sheath for the RC events when the disturbance time is earlier than the ICME start time. Richardson and Cane (2024) provide the details of their identification algorithm with regions initially identified by a low proton T (as compared with the expected temperature based on the speed), then further investigating the intensity, smoothness, and rotation of B, any associated shocks, energetic particle measurements, compositional/charge state measurements, and BDEs. Not all signatures are required for an event to be included in the RC catalog but the authors do indicate whether each event contains the signatures of a FR.
6. *Wind* (Nieves-Chinchilla et al., 2018)—The Wind ICME catalog is another continually-updated list based on Wind observations. It includes an "ICME" start time, a "MO" start time, and a "ICME/MO" end time for each event. We set the ICME time as a sheath/shock time when it differs from the MO time. The MOs were selected for "clear signatures of an organized magnetic structure" in order to facilitate FR reconstructions.

The source catalogs contain CME boundaries based upon in situ observations from either Wind or ACE. Both spacecraft are near Earth so the timing of observed features is typically similar, but not precisely the same. This is particularly true before mid 2004 (i.e., most of our sample) when Wind underwent 67 petal orbits sampling the magnetosphere and several Lissajous orbits before settling into an orbit around L1 (see the orbital trajectory in Figure 1 of Wilson et al., 2021). At its maximum displacement from ACE, roughly 500 earth radii when at L2, an average CME of speed 500 km s^{-1} transient structure would have a time lag of 1.8 hr between the spacecraft. At L1, Wind's orbit still has a larger displacement than ACE, but Rüdisser et al. (2025) show that this causes an average timing difference of only 6.5 min between arrivals at Wind versus other L1 spacecraft.

We note that the LLAMAICE event visualizations also include information from two HSS catalogs (Grandin et al., 2019; Xystouris et al., 2014). We have not analyzed these HSS results in any fashion, we merely show the regions that they have identified as HSS for comparison since the catalogs were readily available and may help interpret the in situ signatures.

2.2. LLAMAICE Catalog and Bounds

After collecting the individual catalogs, the first step is to determine which entries correspond to the same real-world events. Matching entries tend to be straightforward for isolated, clear events. However, CMEs often interact with other CMEs or HSSs before arriving at 1 au, leading to complex in situ signatures. Often at 1 au one can disentangle various features corresponding to different physical structures before the streams fully merge at greater distances (e.g., L. F. Burlaga et al., 1986). We will refer to interacting events as complex systems (CSs), which can be thought of as the progenitors of the largely-merged compound streams observed at farther distances. Decomposing these CSs can be ambiguous, introducing complications with some catalogs treating them as single entries and others breaking them into multiple entries.

We make an initial pass at grouping events using their start times and durations. We then visually inspect the events boundaries overlaid on Wind/ACE data and reassign source catalog events as necessary. This creates a "master list" of LLAMAICE event IDs. During this process we tend to favor identifying long events as a CS and only split them apart with separate LLAMAICE IDs if there is an unambiguous separation between adjacent CMEs. The team confers on these decisions and attempts to remain consistent across events, but it is still a subjective process. Tending toward CS-labeled events means there are many in situ events with a single LLAMAICE ID but multiple sets of boundaries from an individual source catalog.

LLAMACoRe, the first component of the LLAMAVERSE in which LLAMAICE also resides, combined properties from remote reconstruction of CMEs from different source catalogs to get overall values, such as the

average latitude or angular width. While we could also mathematically average the boundary times, the plasma profile at this new time will typically no longer exhibit the specific features expected at a shock/FR boundary. As such, the team inspects each LLAMAICE case and the existing boundaries and comes to a consensus on what they believe to be a new "optimal" set based on the in situ plasma and magnetic field observations. Much like the other catalogs without boundaries defined by quantifiable algorithms, these are still subjective values, which we comment upon further in the discussion. The team tends to use boundaries from existing catalogs as much as possible but will pick a completely new time as needed. This project provides a comprehensive overview for a large number of events, not detailed studies of single cases, so we do not make any micro-adjustments to existing boundaries on the scale of a few minutes. We note that we set all our new boundaries to the timing of Wind observations as more of the source catalogs report Wind times than ACE, but switch to ACE as needed during data gaps. This means that the reported times may differ by a few hours from the arrivals at L1 due to Wind's excursions before mid 2004. We use Wind Solar Wind Experiment (SWE, Ogilvie et al., 1995) and Magnetic Field Investigation (MFI, Lepping et al., 1995) and ACE Solar Wind Electron Proton Alpha Monitor (SWEPAM, McComas et al., 1998) and Magnetometer (MAG, Smith & Ness, 2022) data to examine the magnetic field intensity (B), vector, and angular direction, as well as the proton speed (v), temperature (T), number density (n), and plasma β. We did not consider energetic particles, composition, or BDEs.

We explicitly define the regions we will assign as we believe discrepancies in definitions can explain some of the difference between the boundaries in different catalogs. It is not to say that one particular set of boundaries, including ours, is the "correct" one, just that one should be cautious when comparing across catalogs or selecting a catalog for a specific purpose. We define our regions based upon the plasma and magnetic field in situ signatures and a very generic, idealized picture of a CME, such as the canonical cartoon of Zurbuchen and Richardson (2006). The ejecta can be pictured as curved tube of twisted magnetic field lines, turbulent ambient SW is swept up ahead of it into a sheath or pile-up region, and potentially a CME driven shock at the front of the sheath.

To identify a sheath region, the team looked for a shock/discontinuity across all plasma parameters followed by a turbulent region of enhanced B, n, and T. We also include a sheath region when an event is missing many of the other signatures but does have an obvious enhancement in n ahead of the ejecta and flag these as a pile-up. Many of the front sheath boundaries are proper shocks but others are weaker discontinuities or simply the start of a pile-up region (see, e.g., Salman et al., 2020). Rigorous identification of shocks would be a useful addition to the LLAMAICE catalog but is beyond our current scope. Future revisions to LLAMAICE will incorporate existing shock catalogs, of which numerous are available, such as the Harvard–Smithsonian Center for Astrophysics Interplanetary Shock Database https://lweb.cfa.harvard.edu/shocks/ or the Database of Heliospheric Shock Waves maintained at University of Helsinki https://ipshocks.helsinki.fi/database.

Many people treat the ejecta as a magnetic FR, which would imply a specific set of characteristics for the corresponding in situ observations. These signatures, however, are often not present in the in situ observations. Whether this is due to observational effects (i.e., glancing blows), aging effects, or a misunderstanding of the CME structure itself is of open debate. To avoid existing terminology with precise definitions, such as FR or MC, we will refer to this portion of the in situ signature as the ejecta core (EC). This is the region that exhibits the most FR-like or MC-like characteristics and should correspond to the twisted magnetic field portion of an idealized CME cartoon, regardless of how non-idealized it appears in a real world event.

To identify a EC region, the team looked for relatively smooth rotation in an enhanced B, a smoothly varying v profile (though not necessarily decreasing), as well as low T and β (relative to the sheath or surrounding ambient SW). For cases with a sheath region, we look for a decrease in n relative to the sheath values (but not comparing to the ambient SW). These are the traditional signatures of a FR or MC, but we are not requiring all to be present, simply looking for evidence that this is the main core of the ejecta that we can separate from the ambient SW and any sheath.

Some catalogs, such the RC catalog, include boundaries for both an ICME and a smaller MC within the event. Other catalogs report just a MC, or just an ICME. The distinction between MC/ICME is often made using different signatures, such as compositional/charge state versus magnetic and plasma observations. We focus only on plasma/magnetic field, but find even with only these parameters there are regions within an event that do not fall into our main categories of sheath, EC, or ambient SW. These regions occur between the sheath and EC or between the EC and trailing ambient field and display a mixture of signatures from the adjacent regions. We refer to these as mixed regions (M1/M2 for the front/back), but emphasize that this only implies a mixing of

observational signatures, not necessarily an actual mixing of plasma due to reconnection effects. These are dynamic, propagating structures with regions that evolve for a variety of regions including draping of magnetic field, compression, and reconnection at the boundaries (see, e.g., Kilpua et al., 2013). In many cases, the difference between our EC and mixed regions may be analogous to that of others MC and ICME, but we have not explicitly investigated this for this work. In other cases, these mixed regions correspond to the back portion of an EC that has been altered by the shock of a closely trailing CME.

To identify a mixed region, the team looked for signatures representative of both the sheath and EC (M1) or the EC and ambient SW (M2). For M1 this often means the appearance of rotation in B and/or a decrease in T/β while remaining fairly turbulent. For M2 there is often a discontinuity across multiple parameters and increased turbulence, but the rotation in B and $\beta < 1$ continue for some time before becoming indistinguishable from the ambient SW. We will also use M2 to indicate when the shock from a trailing event clearly disturbs the back portion of the preceding EC, a different form of mixed observations signatures. While including the mixed boundaries helps to more accurately describe the regions within an event, setting precise bounds between mixed and pristine regions is often highly subjective.

LLAMAICE boundaries include up to five boundaries corresponding to four different regions (sheath, M1, EC, M2). We only add LLAMAICE boundaries for events with an identifiable EC region, so our new boundaries have at a minimum an EC start and end time. We will not add boundaries for just a sheath or mixed region encounter, which may differ from the approaches of the source catalogs. The LLAMAICE catalog contains numerous events that exists in one or more source catalog but do not have new LLAMAICE boundaries, either because the team feels it is a ICME encounter that does not sample the EC, the plasma and magnetic field signatures are sufficiently weak such that the team cannot confidently add boundaries, or the team feels the signatures correspond to some other transitory structure (implying a disagreement with that source catalog). We note that team tends toward the conservative side when including the new boundaries, preferring to mistakenly omit a weak case as opposed to erroneously labeling ambient SW or a HSS as an event. Of the 94 cases where the team did not provide new boundaries, 55 of them correspond to events that appear in only one other catalog and 28 appear in only two. We include all source catalogs and any new boundaries in the LLAMAICE catalog so that a user can form their own opinion.

2.3. LLAMAICE Visualizations and Sub-Catalogs

Figure 1 shows an example event from the LLAMAICE catalog. All events are accompanied by a figure in this format, and we have created a Python tool to show this information in an interactive window, which we describe in Supporting Information S1. The LLAMAICE catalog includes both an integer ID and a date ID (YYYY-MM-DD-HHMM), corresponding to the earliest LLAMAICE boundary time. Events without LLAMAICE boundaries are identified by the earliest time in a source catalog. The integer IDs may change in the future as this is a living list, so we encourage use of the date IDs, or to include the LLAMAICE version number with an integer ID. The example in Figure 1 shows event 236 or 2001-08-17T1103. The panels show, from top to bottom, B, B_x, B_y, and B_z in Geocentric Solar Ecliptic (GSE) coordinates, the corresponding latitude (θ) and longitude (ϕ) angle of the GSE B vector, v, T, n, and β. Wind observations are shown in black and ACE in gray. We note that for ϕ we do not connect adjacent points on opposite sides on the 0°/360° circular boundary if they are both within 45° of the boundary.

The source catalog boundaries are shown as vertical, dashed lines with a legend on the right side showing the color associations. We note that there are instances when the catalog boundaries overlap and cannot be distinguished in the figure. This is true for the example shown and numerous events in the LLAMAICE data set. There is no way to visually separate these overlapping bounds without resorting to a variety of line widths and styles that unnecessarily complicate the figure. We note that the Python tool does print text listing all the boundaries, which clearly displays the overlapping times. The LLAMAICE regions are shaded in red, yellow, and blue corresponding to sheath, mixed, and EC, respectively. The top bar above the panels shows the extent of any HSS from those source catalogs as labeled in the legend. We note that these HSS regions are labeled according to their source catalogs with no judgment of their quality from the LLAMAICE team. A LLAMA-style analysis of HSS catalogs would be a worthwhile endeavor. The bottom text shows comments from the LLAMAICE team. Each comment starts with a code indicating the team's confidence in the event being a CME and not some other transient structure. The options are yes (Y), probably yes (PY), maybe (M), and probably not (PN). This is

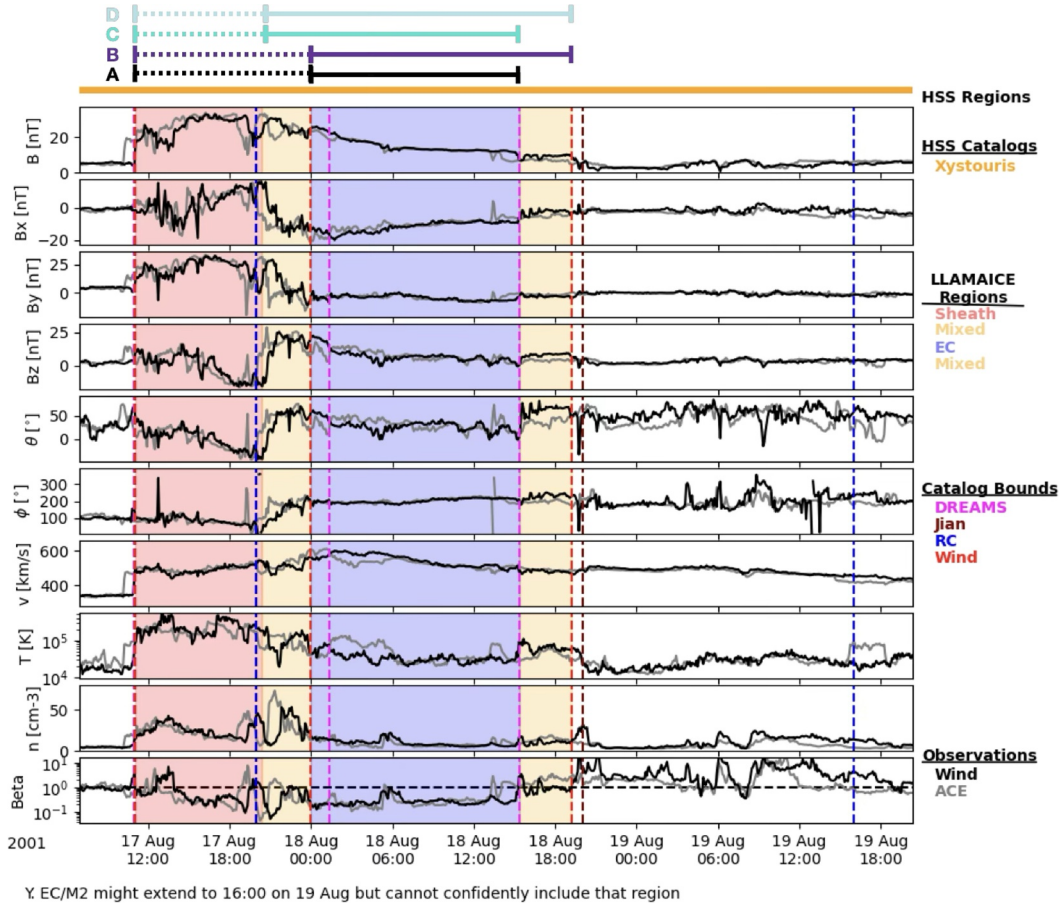

Figure 1. Example of the standard LLAMAICE visualization. The panels show B, B_x, B_y, B_z in GSE coordinates, θ, ϕ, v, T, n, and β from top to bottom. Each panel includes both Wind (black) and ACE (gray) data. The vertical dashed lines show boundaries from the source catalogs, colored according to the legend on the right side. The shaded regions show the bounds determined by the LLAMAICE team, also explained in the legend. The yellow bar at the top represents the times identified as an HSS according to an external catalog. The four bars with endcaps show how the LLAMAICE mixed regions are incorporated into either the sheath (dashed) or EC (solid) region when we compare the LLAMAICE variants with the source catalogs. The bottom of the figure includes comments from the team about the event.

followed by any additional flag codes, which can be complex system (CS), pile-up (PU), small FR in sheath (SFRIS), driverless shock (DLS), shock in ejecta (SIE), and shock in the previous CME (SIP). Not all events will include a flag code and some may have multiple. Following these codes are any comments from the team explaining their decisions or general uncertainties.

We show 2001-08-17T1103 as an arbitrary but fairly clean event that exhibits all four regions. The shock creates an obvious jump in B, v, T, and n and we find that all source catalogs are in relative agreement for this boundary. The source catalogs show a larger spread for both the EC start and end. The RC catalog EC front aligns with the rotational discontinuity in B seen at ACE, the Jian and Wind front aligns with the start of an extended $\beta < 1$ region and less turbulent B, and the DREAMS catalog falls just slightly later when B becomes the most smooth. We interpret this event with M1 starting near the RC boundary (but shifted to Wind data) and ending at the Jian/Wind boundary since the plasma parameters are still enhanced and turbulent but B is beginning to rotate. For the EC end boundary, DREAMS aligns with the return to $\beta > 1$ in the Wind data, Jian/Wind vary slightly from one another but align with the drop in B and T to ambient-like values. The RC includes almost an extra day compared to the other catalogs. We interpret this region as potentially a weak glancing encounter, possibly of a leg. RC include this region because they consider additional parameters such as the charge state, BDEs, and a lower than expected temperature. We assign the LLAMAICE EC end to the DREAMS boundary and add M2 until the Wind boundary since it retains some FR properties but is more turbulent. The comment at the bottom of the figure acknowledges

Table 1
List of the Individual Catalogs Within LLAMAICE

	Name	Time range	nEvents	Sheath	M1	EC	M2
1	CDAW	01/1997–08/2006	59	X	—	X	—
2	DREAMS	02/1995–12/2015	293	X	—	X	—
3	Jian	01/2007–12/2011	229	X	—	X	—
4	Lepping	02/1995–12/2015	105	—	—	X	—
5	RC	05/1996–present	309	X	—	X	—
6	Wind	02/1997–present	219	X	—	X	—
7	LLAMAICEA	02/1995–12/2006	302	X	X	X	X
8	LLAMAICEB	02/1995–12/2006	140	X	X	X	—
9	LLAMAICEC	02/1995–12/2006	137	X	—	X	X
10	LLAMAICED	02/1995–12/2006	80	X	—	X	—

that the region between our M2 and the RC end could potentially be an extension of this event, but the team was not confident enough to incorporate it into our bounds.

This example highlights the importance of a meta-catalog such as LLAMAICE. The team has made an effort to give a best set of boundaries, building upon the knowledge that already exists, but these are still subject to our interpretations. By including multiple interpretations together one can better understand which boundaries are well-known (the shock in this case) and which are more uncertain (all other bounds). We encourage any LLAMAICE users to consider all sets of boundaries before making their own interpretations.

The set of four dashed + solid bars with endcaps has been added just for Figure 1 and is not part of the standard LLAMAICE visualization. In this work, we want to compare LLAMAICE boundaries to those in the source catalogs, but LLAMAICE is the only set with mixed regions. We define four subsets of LLAMAICE labeled A–D, which represent different ways of incorporating the mixed regions into the more limited sheath and FR regime. The bars show which regions are considered sheath (dashed) and EC (solid) when we compare that option to the source catalogs. Option A represents the most pristine FR-like version where we do not include any mixed regions to the EC region. For A, M1 becomes part of the sheath and M2 is dropped. Option B adds M2 to the EC but keeps M1 as part of the sheath. Conversely, option C adds M1 to the EC but excludes M2. Option D represents the most generous interpretation with both M1 and M2 included with EC. All sets of LLAMAICE boundaries will have an A option but may or may not have B–D depending on the presence of M1/M2.

We note that the LLAMAICE visualization will show any previous CMEs (ones that occurred shortly before) or trailing CMEs (ones that occurred shortly after), as appropriate. These will be shown in the same format as the event of interest but the regions will be shaded with lower opacity, all catalog boundaries shown in gray, and a flag added in the legend. We also point out that if using the interactive Python window one can click within a panel and get the corresponding time stamp and *y*-value for that point.

2.4. Catalog Overview

This first LLAMAICE catalog release (v1.0), covering February 1995 through December 2006, contains 1,516 sets of boundaries for 396 events across seven different catalogs (including the LLAMAICE boundaries). If we include the B–D options for LLAMAICE boundaries, the total increases to 1,873 sets of boundaries. Table 1 lists the full time range of each catalog, the number of events included within LLAMAICE v1.0, and the boundaries included for each source catalog. We also include the LLAMAICE A–D options.

Figure 2 shows a visual overview of the complete meta-catalog. Each panel corresponds to a different year (labeled on the *y*-axis) and each line represents the full extent of an event with different colors representing different catalogs. The catalogs appear in the same order from top to bottom in a panel starting with CDAW (orange) then DREAMS (pink), Jian (maroon), Lepping (yellow), RC (blue), Wind (red), and LLAMAICE (black). Multiple events in quick succession can appear as a long continuous line. Solar cycle variations are evident in Figure 2. The maximum of Solar Cycle 23 occurred around 2000–2001 and Figure 2 shows an increase in in situ detections during maximum and the adjacent late-rising and early-declining phases.

3. General Properties

Since we have over 300 events with multiple sets of boundaries, we use LLAMAICE to illustrate how sensitive commonly calculated quantities are to the specific boundaries that are used. In this section we explore the effects on the average plasma properties within the different regions. We seek to compare results between ACE and Wind for every set of catalog boundaries, however, some of Wind's excursions cause it to sample the magnetosphere and both spacecraft experience significant data gaps at various times. Through visual inspection we remove the cases where the Wind B is enhanced (30–100+ nT) and well beyond what is seen at ACE or when there are data gaps of more than a few hours in either set of observations. This leaves us with 297 events with average magnetic

10.1029/2025SW004753

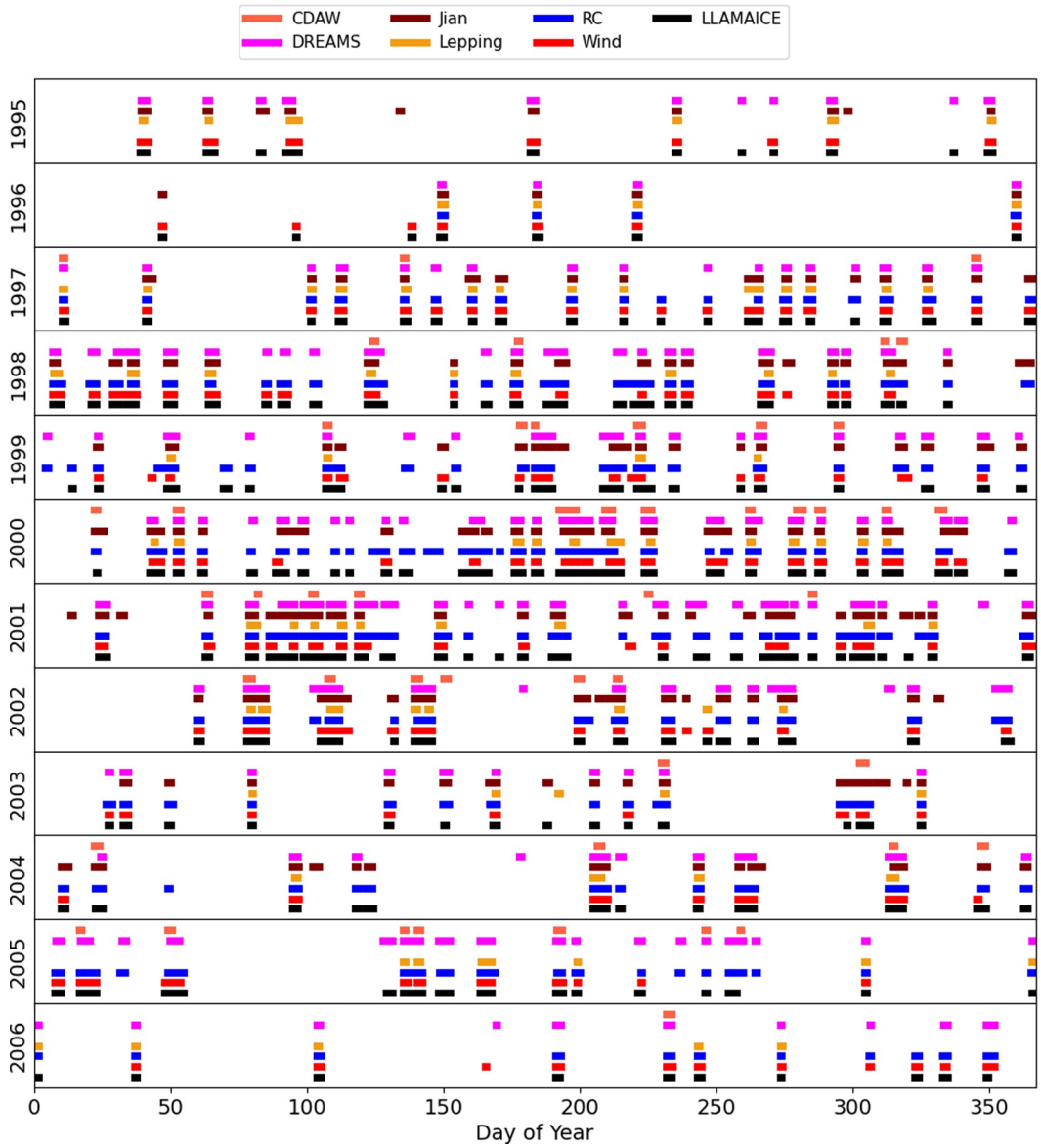

Figure 2. Timeline showing the distribution of events for both the source catalogs and LLAMAICE. Each color represents a different catalog and the lines extend over the full duration of the boundaries (sheath + EC and mixed for LLAMAICE).

field values and 277 with plasma values for the EC region. Not all events have a sheath so we find 239 and 223 events with magnetic and plasma sheath averages.

We acknowledge that to some extent this is an "apples and oranges" comparison, such as using boundaries that may have been based upon Wind with ACE data, or comparing a catalog that selectively isolates pure FR structure versus a more inclusive ICME catalog. This is intentional as such comparisons occur in the field when one does not carefully compare the methodology of different sources. By performing these comparisons over a large data set we aim to quantify the variance one may expect between values reported for different analyses of the same event. We first compare the differences from using different spacecraft, knowing that only one of the two spacecraft is appropriate for each reported set of boundaries. We then compare the effects of boundaries from different source catalogs.

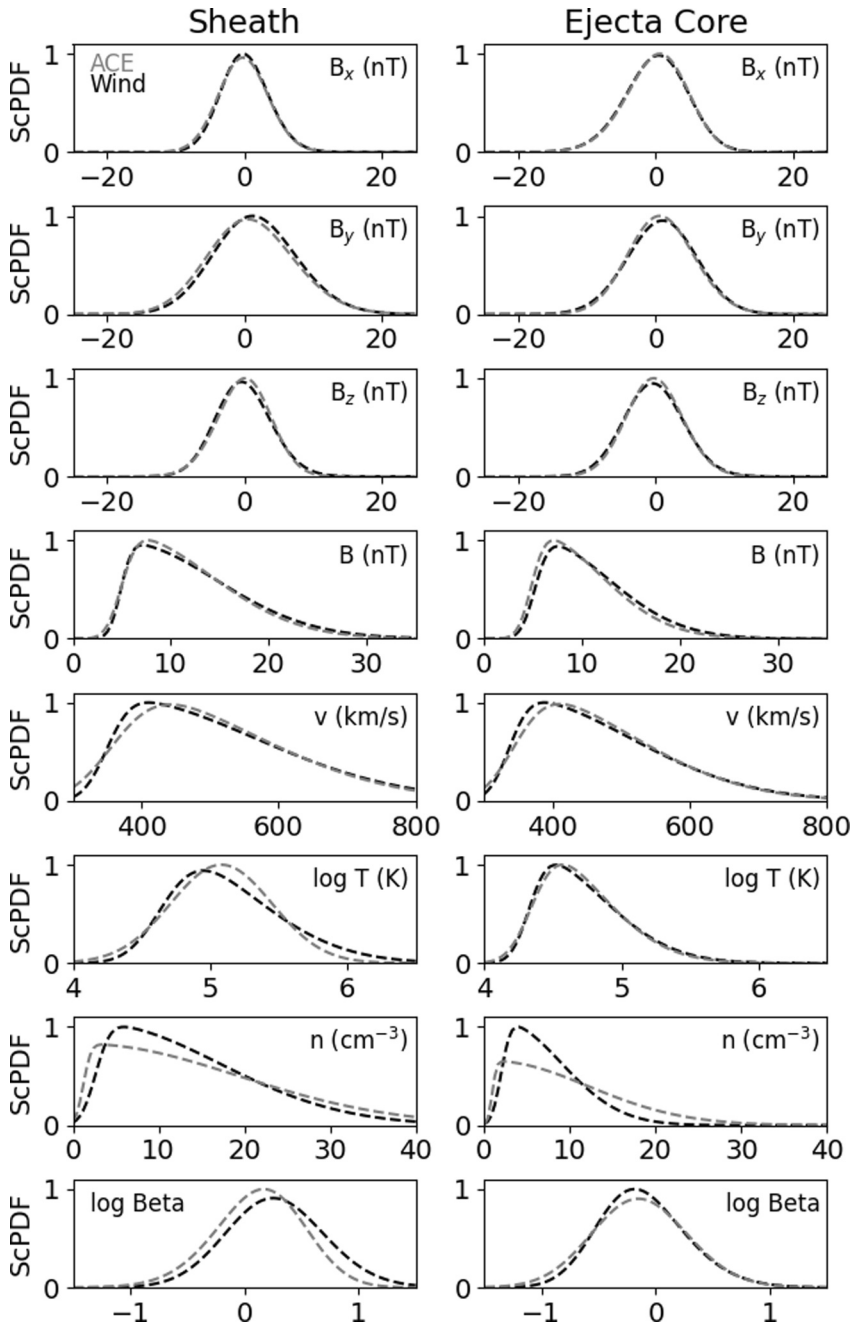

Figure 3. Scaled probability distribution functions (PDFs) for the average properties in the sheath (left) and EC (right) using either Wind (black) or ACE (gray) data. All panels have been normalized such that the overall maximum (from either Wind or ACE) is set to 1.

3.1. ACE/Wind Comparison

For each set of boundaries, we determine the mean values of B_x, B_y, B_z, B, v, log T, n, and log β within the sheath and EC regions using both ACE and Wind 5-min resolution observations. We collect all the values across all catalogs and determine the probability distribution functions (PDFs) for the sheath/EC for each spacecraft. We use a skew normal distribution since many of the parameters exhibit asymmetric profiles. Figure 3 shows scaled versions of these PDFs (ScPDFs) where we have normalized each PDF. We determine the maximum value in the PDFs across all profiles within a panel. This maximum value is then used to normalize all profiles within a panel, which puts all panels on the same *y*-range but keeps the relative distributions the same within a panel. The left

Table 2
ACE/Wind Comparison Metrics

	Sheath					EC				
Parameter	MWU p	MAE	r	R^2 A2W	R^2 A2W	MWU p	MAE	r	R^2 A2W	R^2 A2W
B_x (nT)	0.805	0.90	0.878	0.761	0.748	0.836	0.46	0.978	0.956	0.953
B_y (nT)	0.865	0.96	0.959	0.914	0.905	0.799	0.42	0.983	0.965	0.964
B_z (nT)	0.697	1.03	0.873	0.754	0.737	0.924	0.46	0.976	0.952	0.949
B (nT)	0.802	0.66	0.969	0.938	0.936	0.982	0.36	0.975	0.951	0.948
v (km/s)	0.885	11.17	0.942	0.876	0.888	0.859	5.31	0.997	0.993	0.994
log T (K)	0.046	0.12	0.913	0.728	0.784	0.649	0.08	0.945	0.870	0.889
n (cm^{-3})	0.874	2.18	0.895	0.766	0.798	0.539	1.26	0.890	0.764	0.783
log β	0.014	1.27	0.357	−2.561	0.046	0.313	0.44	0.574	−0.246	0.287

column shows ScPDFs for the sheath region and the right column the EC, with Wind results in black and ACE results in gray. Each panel is labeled with the parameter and its units.

The ScPDFs are quite similar between ACE and Wind for most panels. In addition to the spacecraft not being co-located, these differences result from variations between the individual instruments and how the raw data is processed (e.g., taking moments, fitting Maxwellians) to derive the physical parameters. The strong similarities in Figure 3 show that, on the scale of about 250 events, any effects from the small differences in spacecraft location are largely washed out by both spacecraft sampling from the same distribution of possible sheath/EC properties.

The most significant differences are: (a) a shift in the most probable ACE T to higher values but countered by a weaker tail at the highest values, (b) a broader distribution of densities seen by ACE for both the sheath and EC, and (c) a slightly narrower distribution in the sheath β observed by ACE, accompanied by a slight shift to a lower most probable value. In applying all sets of boundaries to both sets of observations, we are more likely to introduce a misalignment with the ACE data since more source catalogs are Wind-based. This could explain why the sheath has more low density cases for ACE than Wind if the ACE sheaths are more likely to values representative of the EC or ambient SW due to the misalignment. This reasoning, however, would also imply a shift in the ACE temperatures to lower values if it is less likely to contain pure, hot sheath. We observe the opposite, which may suggest a instrumental or processing effect, though we note there is only a minor shift to higher T in the EC.

We support our qualitative comparison between ACE and Wind with more rigorous metrics. Often a t-test is used to compare two different populations. The null hypothesis assumes that the two samples are drawn from the same parent populations and a metric is calculated that determines whether the null hypothesis can be rejected or not. The standard t-test requires that the populations are independent and have a normal distribution with similar variances. Since our distributions exhibit significant skew, we opt for the Mann–Whitney U test (Mann & Whitney, 1947), which provides a similar metric without the assumption of a normal distribution. We calculate the p-value between the ACE and Wind PDFs using the `mannwhitneyu` function from the SciPy stats package. The p-value represents the likelihood that the two distributions come from the same parent population, with a low value (typically below 0.05) suggesting the null hypothesis can be rejected. Table 2 lists the Mann–Whitney U p-values (MWU p) for the sheath and EC in addition to other metrics explained below. We find two statistically-significant values—for the T and β in the sheath with values of 0.046 and 0.014, respectively. β combines the effects of the differences in n, T, and B to produce the most significant differences between the populations observed by ACE and Wind. Every other p-value is well above the critical limit. The lack of any significant difference between ACE and Wind values is an expected result, but good to confirm with quantitative data, particularly when the majority of the Wind observations occur before it arrived at its L1 orbit.

We see essentially no differences in the overall distributions but this does not mean the ACE/Wind values match for individual cases. Figure 4 shows the Wind value versus the ACE value for each parameter for each event. Sheath values are shown in maroon and EC values in blue. The dashed line shows a one-to-one correlation between ACE and Wind. For all parameters we see that the majority cases fall close to the equivalency line and are

10.1029/2025SW004753

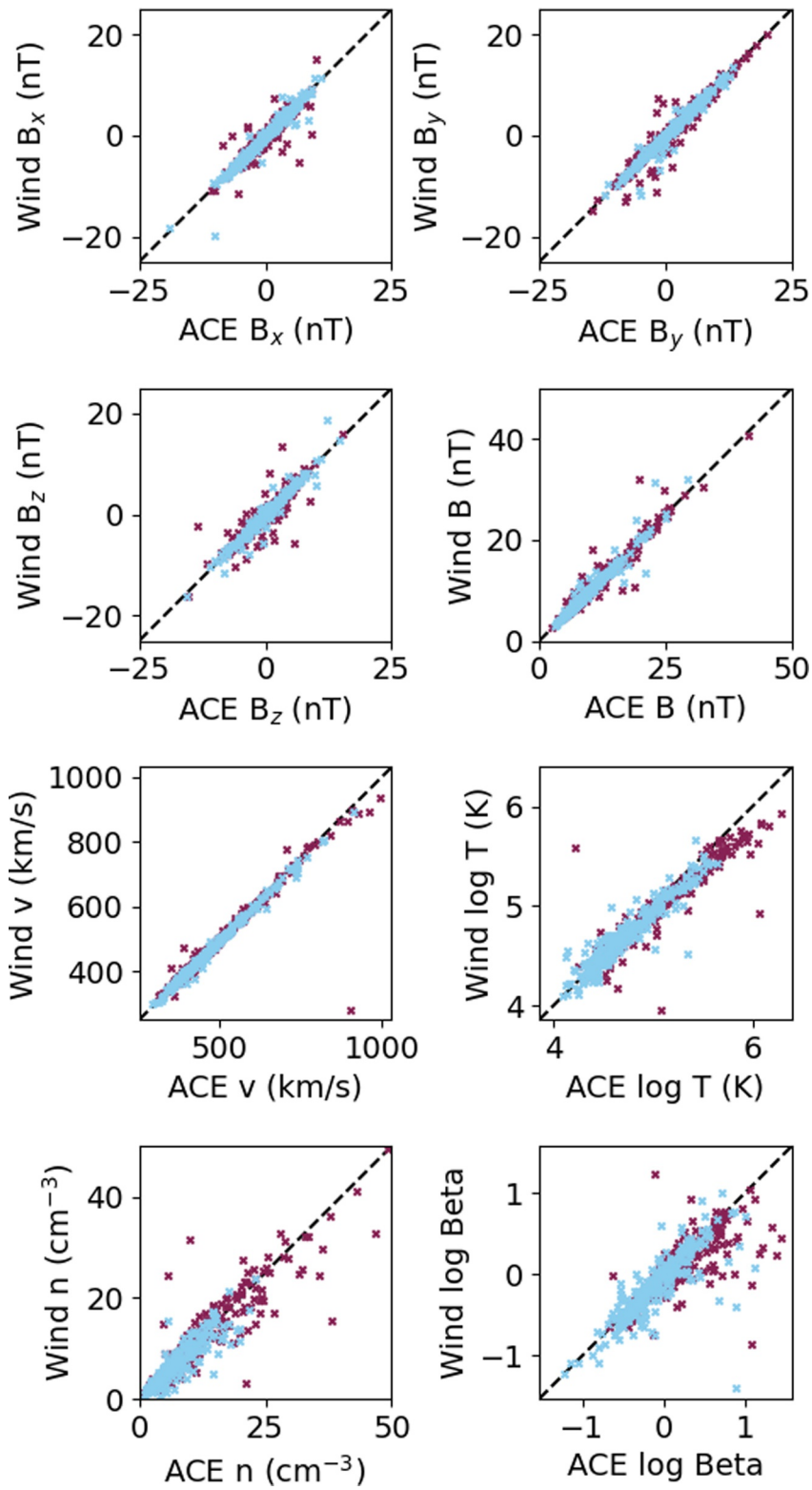

Figure 4. Scatter plot comparing mean values of various properties between Wind and ACE. Sheath values are shown in maroon and EC values in light blue. The dashed line shows a one-to-one equivalency.

highly correlated, but there is some scatter. If the excursion and data gap cases are not excluded this figure includes many more outlier points far from the equivalency line (not shown). There are no systematic variations in the magnetic properties but we do find some in the plasma properties. At high temperatures, the ACE values are consistently higher than Wind values. The populations match below about 10^5 K for both the sheath and EC but have a noticeable shift under the equivalency line that increases as the T increases. We see a similar effect of higher ACE values for the speed above 800 km s^{-1} but it is much weaker and there are fewer events in this regime. The n and β values show the most scatter about the equivalency line. β shows some evidence of the larger values at high values, as would be expected as it is derived from T.

To support this with metrics, for each parameter we calculate the mean absolute error, the correlation coefficient (r), and the coefficient of determination (R-squared/R^2) from ACE to Wind and Wind to ACE, given in Table 2.

The mean absolute error (MAE) is a useful measure that represents the standard uncertainty one can expect for each parameter. Most parameters are strongly correlated, indicating few disagreements between the two spacecraft on whether a parameter has a "small" or "large" value. We do not include the p-values for the correlations as they all show statistical significance well beyond any common limit and are essentially 0. The weakest correlations are the sheath β but even it has p-values of the order 10^{-8}. The R^2 metric is typically used to quantify the amount of variation in a set of observations that can be explained by a model, but we can use it to quantify the variations between ACE and Wind. For example, the ACE to Wind (A2W) values are calculated by treating the ACE values as model results used to explain the "true" Wind values. The resulting number is the fraction of the Wind variation explained by the ACE "model." The R^2 has a maximum value of one for a perfect model and negative values indicate worse performance than assuming a simple model that always returns the mean of the true values. We see positive R^2 for all combinations of parameter, region, and A2W/W2A, except for β. The magnitude of these values varies, with the majority of cases falling between 75% and 90%. We do not see any consistent trends in A2W values being larger or smaller than the W2A values, suggesting that the spacecraft exhibit an equal amount of variation when the excursions and data gaps are accounted for.

3.2. Cross-Catalog Comparison

We now shift to comparing the individual catalogs. One reason for performing such a comparison is because different catalogs are used to validate or even train different space weather models. This is important for both arrival time studies but also for critical parameters such as magnetic field and velocity, and particularly true for machine learning models that require large data sets with easily digestible parameters. While we cannot quantify the effects on the end results of other studies, we can at least look for important differences in the data sets they rely on.

Figure 5 compares the ScPDFs between different catalogs. As we found minimal differences between ACE and Wind in Section 3.1, we only show Wind results. Each panel shows a different parameter with Figure 5a showing results for the sheath and Figure 5b the EC. The legend displays the color for each catalog. Again, the PDFs are normalized using the maximum value in the PDF across all profiles within a panel. Note that we have fewer sheath profiles since the Lepping catalog does not define a sheath region, and we also omit LLAMAICEB and LLAMAICED as they have the same sheath regions as LLAMAICEA and LLAMAICEC, respectively.

The ScPDFs behave fairly similarly across different catalogs, although we see more variation than in the ACE/Wind comparison (Figure 3). Comparing the sheath ScPDFs for different catalogs, we see that most parameters show the same general shape with only a few noticeable variations resulting from the criteria each source catalog uses. B_x and B_y are centered around 0 with slight variations in the distribution widths. The same is true for B_z with the exception of the CDAW catalog (orange) that shows a noticeable shift toward negative B_z. This catalog has the smallest sample size (of the catalogs with sheaths) and focuses on Earth-impacting events, and clearly exhibits some bias toward geoeffective events. We calculate the MWU p-values between distributions and none of the B components have statistically-significant variations, including the CDAW B_z values due to the small sample size. We see some spread in the B distributions with the largest catalogs tending to include more of the low B events and the more selective, smaller catalogs shifted toward higher values. LLAMAICEC (teal) has a more "pure" sheath than LLAMAICEA (black) as it excludes the M1 region. The distributions of the B for these variants peak near the same value, but then we observe a much stronger tail at high values for LLAMAICEC. The variation between CDAW and LLAMAICEA is statistically-significant due to the variations between the most restrictive

10.1029/2025SW004753

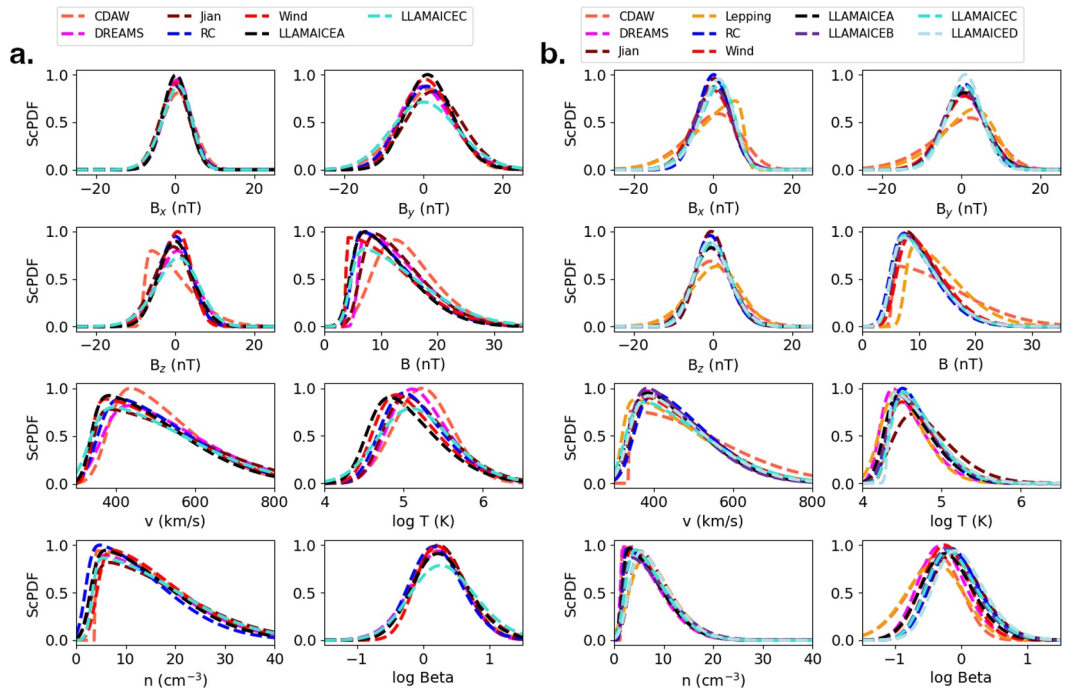

Figure 5. ScPDFs, analogous to Figure 3, but comparing results from different source catalogs. Panel (a) shows results for the sheath and (b) shows results for the FR. Only results using Wind data are shown.

and most inclusive sheath definitions. The CDAW and RC distributions also show statistically significant differences, presumably as ACE observations and the "disturbance time" are not exactly aligned with the Wind observations.

The sheath velocity distributions all have similar tails at the fastest values but more variation in the location of the peak and the probabilities at slow speeds. The CDAW distribution has fewer low speed sheaths and a peak at higher values, which again shows the effects of a smaller catalog focusing on more energetic events. The T distribution shows a significant range in peak locations, likely due to the selection criteria of the individual catalogs. The n distributions are fairly similar to one another. We do see a slight tendency of the RC catalog to include lower n, which we attribute to their boundaries being based on ACE so we have introduced slight sheath misalignment in using them with Wind. Finally, the β distributions show minimal variation, with the exception of LLAMAICEC that includes more high-β values since it is more selective on excluding the M1 region with potential low-β signatures.

The right half of Figure 5 shows the distributions for the EC. The magnetic properties are relatively similar for all catalogs except for CDAW (orange) and Lepping (yellow). These are the smallest two catalogs with the Lepping catalog being even more selective than CDAW as its purpose is to identify regions for which an idealized FR fit can be performed. The CDAW and Lepping catalogs have lower peaks at zero for each of the vector components but broader distributions at strongly positive and strongly negative values. The Lepping catalog shows an unexpected skew toward positive B_x, which is the result of one outlier case in a small sample and using a skewed distribution. The Lepping catalog contains a single entry (2005-05-15T02:10) with an average B_x of -30 nT due to very selective boundaries relative to most other catalogs. All other B_x values are between -10 and 10 nT, so this extreme value throws off the fitted distribution. However, the MWU p value shows that the distribution is not significantly different from the others due to the sample size. In contrast, the more selective nature of the CDAW and Lepping catalogs for stronger events does create statistically-significant distributions for the total B. These two catalogs are not statistically-different from one another, but they are from every other catalog.

The velocity distributions behave very similarly to one another with the exception of the CDAW catalog. The CDAW catalog has a more prevalent tail at high speeds due to favoring more energetic events than the larger catalogs. This variation is statistically significant. The Lepping catalog, despite its small, relatively restrictive

sample, behaves similar to the others, suggesting that its rigorous criteria are more strongly based on the B properties. We find only small shifts in the n distributions with only marginally significant differences between the distributions with the most extreme low (Dreams) and high (Jian) densities.

The T distributions show the most significant variations, both visually in Figure 5 and in terms of the MWU statistics. The CDAW, RC, Wind, and all LLAMAICE variants are similar to one another, but statistically-different from the Dreams, Jian, and Lepping catalogs. Dreams and Lepping are similar to one another with low T but, with the highest T, Jian is statistically different from all other catalogs. These effects, combined with the B and n variations, cause there be noticeable shifts in the β distributions. The visually apparent differences in the figure do correspond to statistically-significant differences.

Overall, we find that different catalogs can produce systematically different variations in the distribution of observed properties in both the sheath and EC. The most significant variations occur for B and T, which also translates into variations in β. These differences result directly from the criteria set by the catalog creators, both in the events included in a catalog and how specific boundaries are selected. This does not provide insight into the physical nature of CMEs so much as the catalogs themselves, but if a researcher is using an existing catalog to constrain results from a physical model they should be cautious about the implications of their chosen catalog.

4. Flux Rope Orientation

We next use LLAMAICE to quantify the sensitivity of reconstructed FR orientations to the chosen EC boundaries. These reconstructions are notoriously sensitive to the chosen boundaries (e.g., Al-Haddad et al., 2013), so LLAMAICE provides a novel opportunity of a large data set that we can use to quantify these variations. Ideally, one should identify what is a proper FR (not just our vague EC region) and only fit that portion, but in practice people pull boundaries from the literature and may not fully consider these details. There are also larger questions of how one should optimally fit a FR. Should the boundaries be fixed so that the model is forced to use the exact start/stop time it has been given or should the model flux rope be allowed to extend beyond them and only fit to the optimal part? If what we refer to as mixed regions exhibit some FR-like behavior should they be included? We emphasize the aim of this section is to better understand the sensitivity of the reconstructions, not to answer the specific questions above or even to provide new values to be blindly used in other studies.

We use every set of EC boundaries within LLAMAICE (again, excluding the Wind excursions and data gaps) and compare the variations between ACE and Wind and across all the source catalogs. This includes using the LLAMAICE subsets with known, systematic variations. We note that we will be introducing error by using catalog boundaries based on Wind timing with ACE measurements, and vice versa, but it is beyond the scope of this work to manually adjust each catalog to the matching features in the alternate spacecraft data. The uncertainties we find between ACE/Wind are a combination of not adjusting the boundaries and the variation in the in situ profiles themselves.

We reconstruct a FR for each set of boundaries using the expansion-modified force-free model (EFF; Farrugia et al., 1993; Yu et al., 2022) used in Palmerio et al. (2025). This code requires the flux rope boundaries and chirality as well as an initial guess of the FR orientation, then employs non-linear least squares minimization from the Python `lmfit` package. The code returns the optimal flux rope inclination/latitude (θ), longitudinal angle (ϕ), impact parameter, axial magnetic field strength, and expansion time (describing the self-similar CME expansion rate). In this work, we will only focus on the axial orientation (θ and ϕ) results.

To automate the FR fitting process, from each set of boundaries and spacecraft we determine the average observed magnetic field vector over an hour in the middle of the time range and set this as our initial guess at the orientation. This will not be the exact center if the CME is expanding, but it is a sufficient approximation. To ensure that the EFF code converges to the overall optimal fit, as opposed to getting stuck in a local minimum, we run it nine times with all combinations of $\theta \in [\theta_0 - 20°, \theta_0, \theta_0 + 20°]$ and $\phi \in [\phi_0 - 30°, \phi_0, \phi_0 + 30°]$, where θ_0 and ϕ_0 represent the initial guess. These $\pm$ values were found to be sufficient offsets to test for convergence through trial and error. The EFF code also requires the handedness of the FR. We explored options using an automatic guess but ultimately found a brute force approach of running both options to work best. From the 18 different iterations of the EFF code, we use the reconstruction with the lowest χ^2 error. We apply this algorithm to every set of EC boundaries for both ACE and Wind, yielding a set of 1,271 reconstructions for each spacecraft.

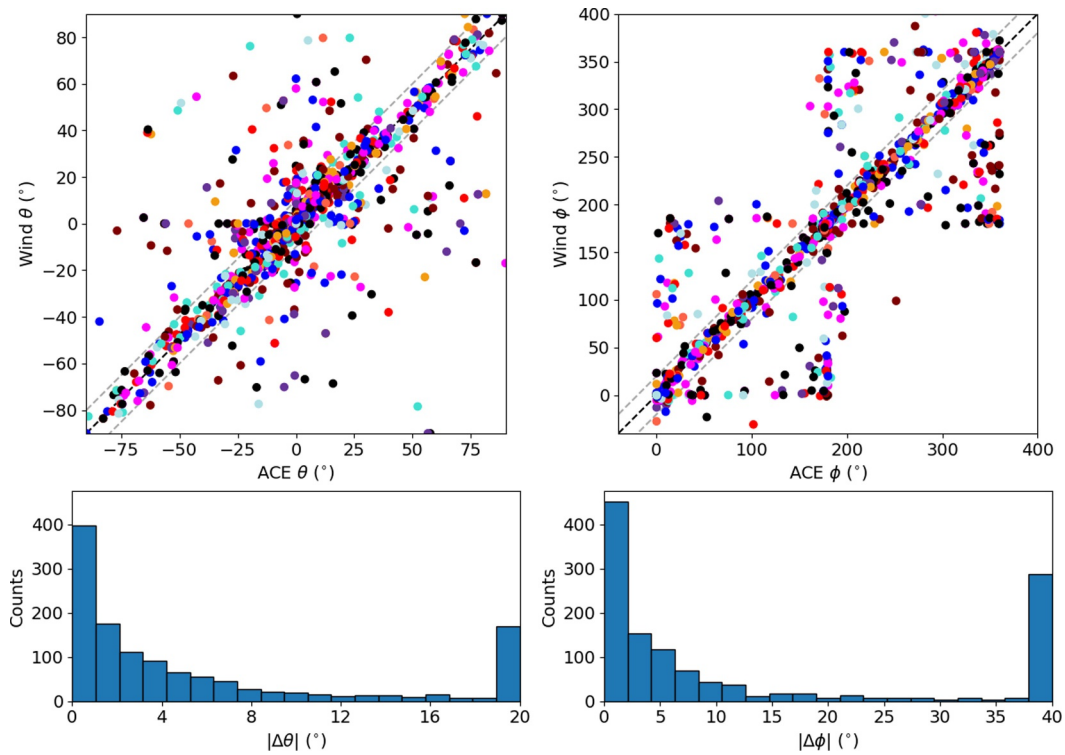

Figure 6. Scatter plots comparing the reconstructed θ (left) and ϕ (right) using either Wind or ACE data. Each point is colored according to its catalog the same as Figure 2 and the dashed line shows a one-to-one equivalency. The bottom panels show histograms of the mean absolute difference between the Wind and ACE values.

4.1. Comparison of Discrete Properties

Before comparing θ and ϕ, we consider the handedness and general inclination of the reconstructions. We categorize each fit as low ($\theta \leq 35°$), moderate ($35° < \theta < 55°$), or high-inclination ($\theta \geq 55°$), using the same ranges as Palmerio et al. (2018). We only find matching handedness between ACE and Wind 77.2% of the time (982 events), highlighting how sensitive these reconstructions can be. The general inclination tends to be more consistent with 92.4% of cases (1,175 events) in agreement for whether an event is low, moderate, or high inclination. We note that the data set is heavily weighted toward low inclination events for both ACE and Wind (roughly 90% compared to 5% for each of the other categories).

We also compare these properties between the different catalogs for the same event. Using Wind observations, we have 264 events with multiple sets of boundaries. Only 123 of these (46.6%) have a consistent handedness across all reconstructions, though an additional 62 (23.5%) have three or more sets of boundaries and only one reconstruction with a differing handedness. The general inclination varies more between catalogs than in the ACE/Wind comparison with 160 events (60.6%) fully consistent and 49 "one-off" cases (18.5%). We find similar metrics for the ACE-based reconstructions.

4.2. Comparison of Orientation

We now compare the numerical variation between different reconstructions of the orientation. Figure 6 compares the Wind- and ACE-based reconstructed θ (left panels) and ϕ (right panels) for every set of boundaries. The top panels show a scatter plot where each point is colored according to the source catalog in the same manner as Figure 5. In addition to the dashed, black one-to-one equivalency line we include dashed gray lines at differences of $\pm 10°$ for $\Delta\theta$ and $\pm 20°$ for $\Delta\phi$. The bottom panels show a histogram of the absolute difference between the ACE and Wind values ($\Delta\theta$ and $\Delta\phi$).

In the scatter plot panels, the majority of points fall close the dashed one-to-one equivalency line, but we also see a lot of scatter. The ϕ panel exhibits two box-like features due to the reconstruction model favoring orientations of

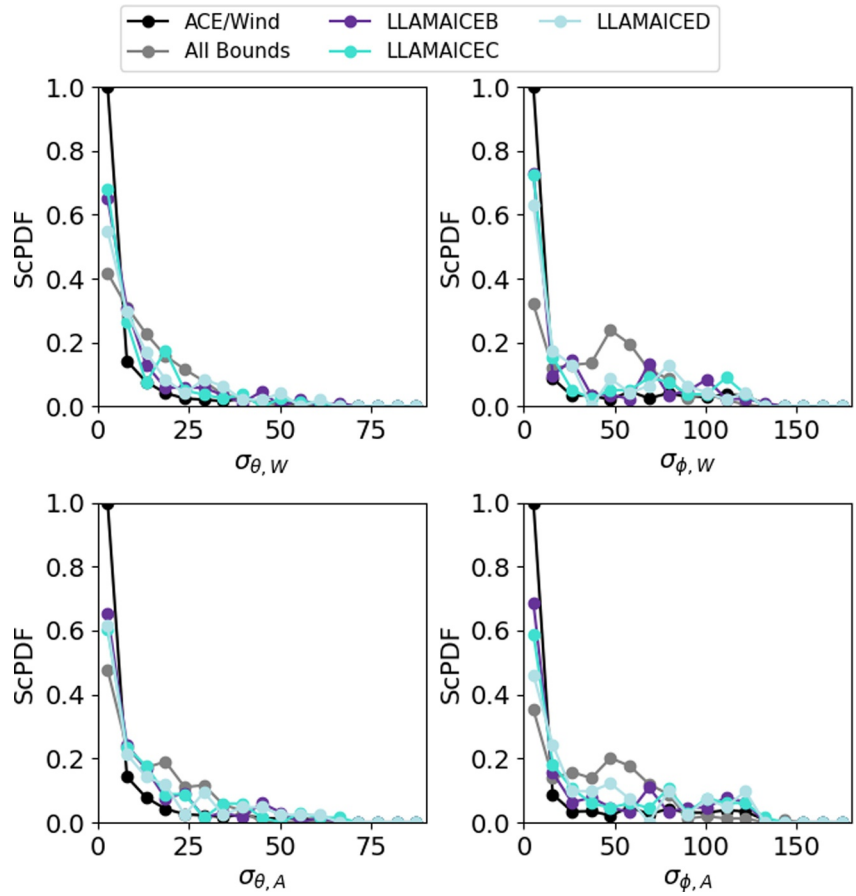

Figure 7. Scaled PDFs of the standard deviation, σ, in θ (left) and ϕ (right) for both Wind (top) and ACE (bottom). The black line shows the σ in the reconstructed values when using the same boundaries but comparing ACE/Wind. The gray line shows σ across all boundaries for a single event. The remaining colored lines compare LLAMAICEA values with those from one of the other variants (LLAMAICEB, LLAMAICEC, or LLAMAICED).

0°, 180°, and 360°. These tend to be the values that minimize the error when the model is not quickly converging to a good fit. Similarly, the θ panel shows increased density around the $\theta = 0°$ lines, but this is less prominent than the ϕ effect. We note that we have accounted for the circular nature of ϕ and visualize points such that the difference between the ACE/Wind values is always less than 180°, which is why there are some points below 0° and above 360°.

The histograms confirm that most reconstructions are in close agreement between ACE and Wind. We truncate the range of the histograms due to the limited number of cases at higher values. We find 64.5% of cases have a $\Delta\theta$ less than 5° and 78.8% are less than 10°. For $\Delta\phi$ we find 51.1%, 65.0%, and 72.4% for limits of 5°, 10°, and 20°. The median differences are 2.7° for $\Delta\theta$ and 4.8° for $\Delta\phi$. We infer that in most cases the difference between the ACE and Wind in situ profiles only cause minor variations in the reconstruction of the orientation, but there is still a significant population where the variation is much larger. We have not investigated whether the larger variations can be attributed to the 2 hr or less differences in the time of arrival at the different spacecraft locations (most catalogs are Wind-based) or if the profiles are significantly different beyond a temporal shift.

For each event we compare variation in the orientation across the different sets of boundaries. For each case with two or more sets of boundaries, we calculate the standard deviation, σ, in θ and ϕ. Figure 7 shows the ScPDF of σ for different data sets. The top and bottom rows show Wind and ACE values and the left and right columns show θ and ϕ. The black line represents the ACE/Wind comparison, which is equivalent to the histograms in Figure 6 divided by $\sqrt{2}$ to convert from an absolute difference to the standard deviation between two points. The gray line represents the standard deviation between all sets of boundaries for each event. The three colored lines represent

comparisons between LLAMAICEA and one of the three other LLAMAICE variants (B, C, or D) as indicated in the legend.

The ACE/Wind comparison (black) has the highest ScPDF at low values of σ indicating those reconstructions tend to be the most similar. The set of all bounds (gray) tends to have the largest values of σ across all panels. If we compare the median value of all σ over the full sample we see the all bounds values are about 4 times higher than the ACE/Wind for the inclination—9.8° within Wind and 10.3° within ACE versus 2.3° for ACE versus Wind (converting the ACE/Wind difference between two values to σ and using only the multi-catalog events). The cross-catalog variations are roughly 10 times larger than the spacecraft comparison for the longitudinal angle (43.0° and 37.5° compared to 3.4°). We see a peak in all bounds for the ϕ distributions near 50° for which we have no explanation, but note this would be close to σ calculated if one has two points differing by 90°. We do not see that significant of a difference between the LLAMAICE variants despite their boundaries having known, systematic variations. There is a slight hint at LLAMAICED having the largest variations from LLAMAICEA, which makes sense as it incorporates both of the mixed regions into the FR reconstruction. The ACE results suggest that LLAMAICEB is more similar to LLAMAICEA than LLAMAICEC, suggesting that including the back mixed region into the FR causes less changes than including the front mixed region, but this is not evident in the Wind profiles. Overall, we see that the variation between different catalogs is more significant than the variation from using different spacecraft data, but cannot conclude anything about the specific factors influencing the variation between catalogs.

5. Discussion

We have presented a new meta-catalog collecting the existing repositories of near-Earth in situ CME boundaries. From this collection we have added our own new set of informed boundaries, building upon the existing information. Each event was initially looked at by all team members individually, followed by the team meeting together to discuss extensively and come to a consensus on the boundaries. Our team believes that our sets of boundaries are "best" and represent the criteria we set when establishing our catalog. We also acknowledge that every group responsible for one of the source catalogs likely believed the same about their own work. We emphasize that the power of LLAMAICE is in the collection of results, which should enable the community to better make their own informed decisions. We do not suggest that any set of boundaries from the literature, including our own, should be thought of as the standard and preferred choice for any specific research project. Rather, it is critical to look at what factors were considered when forming a catalog and decide whether it is a suitable match to a particular use case. This warning extends beyond just in situ boundary catalogs and we encourage more thoughtful use of any catalogs readily available on the internet or within the literature.

This work has combined catalogs based on in situ observations from both ACE and Wind, which were not co-located at L1 for much of this time period. The physical separation of up to 0.01 au correspond to time lags of roughly 2 hr (assuming basic kinematic propagation of a 500 km s^1 structure). The spacecraft are not necessarily radially aligned, so it is likely that each samples slightly different portions of a CME. In situ measurements represent a single path through a CME. The community is just starting to understand the scales upon which variations occur. The basic comparisons in this work show that ACE and Wind are largely sampling the same distributions of CME properties, but there are often non-negligible variations on a case by case basis. The recent conjunction of STEREO-A with L1 spacecraft provided an opportunity to study the meso-scale structure of CMEs (e.g., Banu et al., 2025; Lugaz et al., 2024) over a range of separations and has reinforced the idea that single-pass measurements may not be representative of the global structure. We believe that the single-spacecraft measurements can still be useful, especially when we do not have consistent multi-point measurements sampling a range of scales, but we caution the community to be aware of the uncertainties and not overly emphasize the significance of the results.

6. Conclusion

LLAMAICE combines existing catalogs to create a new meta-catalog with 1,516 sets of in situ CME boundaries for 396 unique events between February 1995 and December 2006. Catalogs define their boundaries using a variety of different signatures, which can cause misalignments between what different catalogs report as a CME boundary. Other times, the signatures themselves may just be confusing with portions displaying characteristics representative of multiple region types. In addition to collating the existing catalogs, the LLAMAICE team has

developed a new set of boundaries, building upon the existing work and adding additional mixed regions between the sheath and ejecta core (EC) front and the EC end and the ambient SW to account for some of the various observed phenomena. These mixed regions represent specifically a mixture of signatures and not necessarily a mixture of plasma, though that is one possible interpretation in addition to compression, magnetic draping, and other evolutionary effects. In some instances the mixed regions may reflect the difference between what is typically labeled an ICME versus a magnetic cloud.

LLAMAICE's collection of boundaries provides an opportunity to explore how sensitive derived results are to a chosen catalog or spacecraft observations. We illustrated two such studies: (a) a comparison of the average properties within the sheath and EC regions, and (b) a comparison of reconstructed orientations. For both studies we see more variation across different boundaries of the catalogs than we do from switching between using either Wind or ACE data. These large statistics corroborate the smaller-sample results obtained by Lugaz et al. (2018) and Ala-Lahti et al. (2020), who determined the typical scales of magnetic coherence between ACE and Wind measurements for ECs and sheaths, respectively. Comparing the mean sheath and EC properties across the different catalogs, we find the largest variations occur for the total magnetic field strength and temperature and are a direct result of the criteria used to define the boundaries. The smaller catalogs tend to focus on more energetic events, which can lead to biases in the distributions of their properties relative to the larger, more inclusive catalogs.

Finally, we quantify the generally-known limitations of in situ CME reconstructions. The reconstructions maintain the same handedness 77% of the time when one switches between ACE and Wind data. This decreases to 47% when one compares different catalogs using the same spacecraft data, though an additional 29% have three or more sets of boundaries and only one set in disagreement. We also consider the general inclination (e.g., low, moderate, or high) and find more consensus than for the handedness. The general inclination agrees 92% of the time between spacecraft and 61% across catalogs (with 19% "one-off"). We further quantify the variation in orientation, finding relatively small median deviations between ACE and Wind (2.7° in inclination and 4.8° in longitude) but note a significant number of extreme outliers. Compared to the cross-spacecraft variation, the cross-catalog variation is about 4 times larger for the inclination and 10 times larger for the longitudinal angle. While still useful, we suggest relatively large uncertainties be adopted for any single-encounter in situ CME FR reconstruction.

The two studies in this work are examples of the types of analysis that can be performed with a meta-catalog such as LLAMAICE. We encourage the community to use this data set for additional meta-catalog analysis, helping build our understanding of how the subtle differences between catalogs can significant implications on scientific research.

Conflict of Interest

The authors declare no conflicts of interest relevant to this study.

Availability Statement

The present version of LLAMAICE and future updates to the meta-catalog can be accessed at osprei.space/llamaice The LLAMAICE data and the script for visualizing events is available via GitHub at github.com/ckay314/LIviewer and has been archived via Zenodo (Kay, 2026a). In Supporting Information S1 includes text files with the new LLAMAICE boundaries, the source catalog boundaries, and everything integrated into a single list of boundaries. We also provided files with the mean sheath/FR properties and the reconstructed FR orientations. All data files have been archived at Zenodo (Kay, 2026b).

Acknowledgments
First and foremost we acknowledge the authors and teams responsible for compiling the individual catalogs that comprise LLAMAICE. None of this work would have been possible without these existing sources. C. Kay was funded by internal investment within the APL Space Exploration Sector. E. Palmerio acknowledges support from NASA's Heliophysics Guest Investigators-Open (Grant 80NSSC23K0447) and Living With a Star (Grant 80NSSC24K1108) programs. K.M. and M.D. acknowledge funding from the ESA project No. 4000146956/24/NL/MH/mp. M.D. acknowledges funding from the European Union's Horizon Europe programme under grant agreement No 101135044 (project SPEARHEAD). E.E. D, H.T.R, E.W. and C.M. are supported by ERC grant (HELIO4CAST, 10.3030/101042188). Funded by the European Union. Views and opinions expressed are however those of the author(s) only and do not necessarily reflect those of the European Union, the European Research Council Executive Agency or the European Health and Digital Executive Agency (HaDEA). Neither the European Union nor the granting authorities can be held responsible for them.

References

Aguilar-Rodriguez, E., Blanco-Cano, X., & Gopalswamy, N. (2006). Composition and magnetic structure of interplanetary coronal mass ejections at 1 AU. *Advances in Space Research*, *38*(3), 522–527. https://doi.org/10.1016/j.asr.2005.01.051

Ala-Lahti, M., Ruohotie, J., Good, S., Kilpua, E. K. J., & Lugaz, N. (2020). Spatial coherence of interplanetary coronal mass ejection sheaths at 1 AU. *Journal of Geophysical Research: Space Physics*, *125*(9), e2020JA028002. https://doi.org/10.1029/2020JA028002

Al-Haddad, N., & Lugaz, N. (2025). The magnetic field structure of coronal mass ejections: A more realistic representation. *Space Science Reviews*, *221*(1), 12. https://doi.org/10.1007/s11214-025-01138-w

Al-Haddad, N., Nieves-Chinchilla, T., Savani, N. P., Lugaz, N., & Roussev, I. I. (2018). Fitting and reconstruction of thirteen simple coronal mass ejections. *Solar Physics*, *293*(5), 73. https://doi.org/10.1007/s11207-018-1288-3

Al-Haddad, N., Nieves-Chinchilla, T., Savani, N. P., Möstl, C., Marubashi, K., Hidalgo, M. A., et al. (2013). Magnetic field configuration models and reconstruction methods for interplanetary coronal mass ejections. *Solar Physics*, *284*(1), 129–149. https://doi.org/10.1007/s11207-013-0244-5

Al-Haddad, N., Poedts, S., Roussev, I., Farrugia, C. J., Yu, W., & Lugaz, N. (2019). The magnetic morphology of magnetic clouds: Multi-spacecraft investigation of twisted and writhed coronal mass ejections. *The Astrophysical Journal*, *870*(2), 100. https://doi.org/10.3847/1538-4357/aaf38d

Banu, S. A., Lugaz, N., Zhuang, B., Al-Haddad, N., Farrugia, C. J., & Galvin, A. B. (2025). Investigating coronal mass ejections through multispacecraft measurements: STEREO-A and L1 in 2022–2023. *The Astrophysical Journal*, *982*(1), 47. https://doi.org/10.3847/1538-4357/adb60c

Burlaga, L., Sittler, E., Mariani, F., & Schwenn, R. (1981). Magnetic loop behind an interplanetary shock—Voyager, Helios, and IMP 8 observations. *Journal of Geophysical Research*, *86*(A8), 6673–6684. https://doi.org/10.1029/JA086iA08p06673

Burlaga, L. F., McDonald, F. B., & Schwenn, R. (1986). Formation of a compound stream between 0.85 AU and 6.2 AU and its effects on solar energetic particles and galactic cosmic rays. *Journal of Geophysical Research*, *91*(A12), 13331–13340. https://doi.org/10.1029/JA091iA12p13331

Chi, Y., Shen, C., Wang, Y., Xu, M., Ye, P., & Wang, S. (2016). Statistical study of the interplanetary coronal mass ejections from 1995 to 2015. *Solar Physics*, *291*(8), 2419–2439. https://doi.org/10.1007/s11207-016-0971-5

Colaninno, R. C., & Vourlidas, A. (2015). Using multiple-viewpoint observations to determine the interaction of three coronal mass ejections observed on 2012 March 5. *The Astrophysical Journal*, *815*(1), 70. https://doi.org/10.1088/0004-637X/815/1/70

Dasso, S., Nakwacki, M. S., Démoulin, P., & Mandrini, C. H. (2007). Progressive transformation of a flux rope to an ICME. Comparative analysis using the direct and fitted expansion methods. *Solar Physics*, *244*(1–2), 115–137. https://doi.org/10.1007/s11207-007-9034-2

Davies, E. E., Forsyth, R. J., Good, S. W., & Kilpua, E. K. J. (2020). On the radial and longitudinal variation of a magnetic cloud: ACE, Wind, ARTEMIS and Juno Observations. *Solar Physics*, *295*(11), 157. https://doi.org/10.1007/s11207-020-01714-z

Davies, E. E., Möstl, C., Owens, M. J., Weiss, A. J., Amerstorfer, T., Hinterreiter, J., et al. (2021). In situ multi-spacecraft and remote imaging observations of the first CME detected by Solar Orbiter and BepiColombo. *Astronomy & Astrophysics*, *656*, A2. https://doi.org/10.1051/0004-6361/202040113

Domingo, V., Fleck, B., & Poland, A. I. (1995). The SOHO Mission: An overview. *Solar Physics*, *162*(1–2), 1–37. https://doi.org/10.1007/BF00733425

Eddy, J. A. (1974). A nineteenth-century coronal transient. *Astronomy & Astrophysics*, *34*, 235.

Farrugia, C. J., Burlaga, L. F., Osherovich, V. A., Richardson, I. G., Freeman, M. P., Lepping, R. P., & Lazarus, A. J. (1993). A study of an expanding interplanatary magnetic cloud and its interaction with the Earth's magnetosphere—The interplanetary aspect. *Journal of Geophysical Research*, *98*(A5), 7621–7632. https://doi.org/10.1029/92JA02349

Gopalswamy, N., Xie, H., Mäkelä, P., Akiyama, S., Yashiro, S., Kaiser, M. L., et al. (2010). Interplanetary shocks lacking type II radio bursts. *The Astrophysical Journal*, *710*(2), 1111–1126. https://doi.org/10.1088/0004-637X/710/2/1111

Gosling, J. T., Bame, S. J., McComas, D. J., & Phillips, J. L. (1990). Coronal mass ejections and large geomagnetic storms. *Geophysical Research Letters*, *17*(7), 901–904. https://doi.org/10.1029/GL017i007p00901

Grandin, M., Aikio, A. T., & Kozlovsky, A. (2019). Properties and geoeffectiveness of solar wind high-speed streams and stream interaction regions during solar Cycles 23 and 24. *Journal of Geophysical Research: Space Physics*, *124*(6), 3871–3892. https://doi.org/10.1029/2018JA026396

Hu, Q., & Sonnerup, B. U. Ö. (2002). Reconstruction of magnetic clouds in the solar wind: Orientations and configurations. *Journal of Geophysical Research*, *107*(A7), 1142. https://doi.org/10.1029/2001JA000293

Huttunen, K. E. J., Schwenn, R., Bothmer, V., & Koskinen, H. E. J. (2005). Properties and geoeffectiveness of magnetic clouds in the rising, maximum and early declining phases of solar cycle 23. *Annales Geophysicae*, *23*(2), 625–641. https://doi.org/10.5194/angeo-23-625-2005

Jian, L., Russell, C. T., Luhmann, J. G., & Skoug, R. M. (2006). Properties of interplanetary coronal mass ejections at one AU during 1995 2004. *Solar Physics*, *239*(1–2), 393–436. https://doi.org/10.1007/s11207-006-0133-2

Kaiser, M. L., Kucera, T. A., Davila, J. M., St. Cyr, O. C., Guhathakurta, M., & Christian, E. (2008). The STEREO mission: An introduction. *Space Science Reviews*, *136*(1–4), 5–16. https://doi.org/10.1007/s11214-007-9277-0

Kay, C. (2026a). Llamaice viewer. *Zenodo*. https://doi.org/10.5281/zenodo.18260710

Kay, C. (2026b). Supporting files for "collection, collation, and comparison of near-Earth in situ CME boundaries". *Zenodo*. https://doi.org/10.5281/zenodo.18260760

Kay, C., Opher, M., & Evans, R. M. (2015). Global trends of CME deflections based on CME and solar parameters. *The Astrophysical Journal*, *805*(2), 168. https://doi.org/10.1088/0004-637X/805/2/168

Kay, C., & Palmerio, E. (2024). Collection, collation, and comparison of 3D coronal CME reconstructions. *Space Weather*, *22*(1), e2023SW003796. https://doi.org/10.1029/2023SW003796

Kilpua, E. K. J., Isavnin, A., Vourlidas, A., Koskinen, H. E. J., & Rodriguez, L. (2013). On the relationship between interplanetary coronal mass ejections and magnetic clouds. *Annales Geophysicae*, *31*(7), 1251–1265. https://doi.org/10.5194/angeo-31-1251-2013

Kilpua, E. K. J., Koskinen, H. E. J., & Pulkkinen, T. I. (2017). Coronal mass ejections and their sheath regions in interplanetary space. *Living Reviews in Solar Physics*, *14*(1), 5. https://doi.org/10.1007/s41116-017-0009-6

Klein, L. W., & Burlaga, L. F. (1982). Interplanetary magnetic clouds at 1 AU. *Journal of Geophysical Research*, *87*(A2), 613–624. https://doi.org/10.1029/JA087iA02p00613

Lepping, R. P., Acũna, M. H., Burlaga, L. F., Farrell, W. M., Slavin, J. A., Schatten, K. H., et al. (1995). The wind magnetic field investigation. *Space Science Reviews*, *71*(1–4), 207–229. https://doi.org/10.1007/BF00751330

Lepping, R. P., Berdichevsky, D. B., Wu, C. C., Szabo, A., Narock, T., Mariani, F., et al. (2006). A summary of WIND magnetic clouds for years 1995–2003: Model-fitted parameters, associated errors and classifications. *Annales Geophysicae*, *24*(1), 215–245. https://doi.org/10.5194/angeo-24-215-2006

Lepping, R. P., Burlaga, L. F., & Jones, J. A. (1990). Magnetic field structure of interplanetary magnetic clouds at 1 AU. *Journal of Geophysical Research*, *95*(A8), 11957–11965. https://doi.org/10.1029/JA095iA08p11957

Lepping, R. P., Wu, C. C., Berdichevsky, D. B., & Szabo, A. (2020). Model fitting of wind magnetic clouds for the period 2004–2006. *Solar Physics*, *295*(6), 83. https://doi.org/10.1007/s11207-020-01630-2

Lugaz, N., Farrugia, C. J., Winslow, R. M., Al-Haddad, N., Galvin, A. B., Nieves-Chinchilla, T., et al. (2018). On the spatial coherence of magnetic ejecta: Measurements of coronal mass ejections by multiple spacecraft longitudinally separated by 0.01 au. *The Astrophysical Journal Letters*, *864*(1), L7. https://doi.org/10.3847/2041-8213/aad9f4

Lugaz, N., Temmer, M., Wang, Y., & Farrugia, C. J. (2017). The interaction of successive coronal mass ejections: A review. *Solar Physics*, *292*(4), 64. https://doi.org/10.1007/s11207-017-1091-6

Lugaz, N., Zhuang, B., Scolini, C., Al-Haddad, N., Farrugia, C. J., Winslow, R. M., et al. (2024). The width of magnetic ejecta measured near 1 AU: Lessons from STEREO-A measurements in 2021–2022. *The Astrophysical Journal*, *962*(2), 193. https://doi.org/10.3847/1538-4357/ad17b9

Lynch, B. J., Al-Haddad, N., Yu, W., Palmerio, E., & Lugaz, N. (2022). On the utility of flux rope models for CME magnetic structure below 30 R⊙. *Advances in Space Research*, *70*(6), 1614–1640. https://doi.org/10.1016/j.asr.2022.05.004

Lynch, B. J., Zurbuchen, T. H., Fisk, L. A., & Antiochos, S. K. (2003). Internal structure of magnetic clouds: Plasma and composition. *Journal of Geophysical Research*, *108*(A6), 1239. https://doi.org/10.1029/2002JA009591

Mann, H. B., & Whitney, D. R. (1947). On a test of whether one of two random variables is stochastically larger than the other. *The Annals of Mathematical Statistics*, *18*(1), 50–60. https://doi.org/10.1214/aoms/1177730491

McComas, D. J., Bame, S. J., Barker, P., Feldman, W. C., Phillips, J. L., Riley, P., & Griffee, J. W. (1998). Solar wind electron proton alpha monitor (SWEPAM) for the advanced composition explorer. *Space Science Reviews*, *86*(1–4), 563–612. https://doi.org/10.1023/A:1005040232597

Millward, G., Biesecker, D., Pizzo, V., & de Koning, C. A. (2013). An operational software tool for the analysis of coronagraph images: Determining CME parameters for input into the WSA-Enlil heliospheric model. *Space Weather*, *11*(2), 57–68. https://doi.org/10.1002/swe.20024

Möstl, C., Farrugia, C. J., Temmer, M., Miklenic, C., Veronig, A. M., Galvin, A. B., et al. (2009). Linking remote imagery of a coronal mass ejection to its in situ signatures at 1 AU. *The Astrophysical Journal Letters*, *705*(2), L180–L185. https://doi.org/10.1088/0004-637X/705/2/L180

Mulligan, T., Reinard, A. A., & Lynch, B. J. (2013). Advancing in situ modeling of ICMEs: New techniques for new observations. *Journal of Geophysical Research: Space Physics*, *118*(4), 1410–1427. https://doi.org/10.1002/jgra.50101

Nieves-Chinchilla, T., Vourlidas, A., Raymond, J. C., Linton, M. G., Al-haddad, N., Savani, N. P., et al. (2018). Understanding the internal magnetic field configurations of ICMEs using more than 20 years of wind observations. *Solar Physics*, *293*(2), 25. https://doi.org/10.1007/s11207-018-1247-z

Ogilvie, K. W., Chornay, D. J., Fritzenreiter, R. J., Hunsaker, F., Keller, J., Lobell, J., et al. (1995). SWE, a comprehensive plasma instrument for the wind spacecraft. *Space Science Reviews*, *71*(1–4), 55–77. https://doi.org/10.1007/BF00751326

Ogilvie, K. W., & Desch, M. D. (1997). The wind spacecraft and its early scientific results. *Advances in Space Research*, *20*(4–5), 559–568. https://doi.org/10.1016/S0273-1177(97)00439-0

Owens, M. J., Lockwood, M., & Barnard, L. A. (2017). Coronal mass ejections are not coherent magnetohydrodynamic structures. *Scientific Reports*, *7*(1), 4152. https://doi.org/10.1038/s41598-017-04546-3

Palmerio, E., Carcaboso, F., Khoo, L. Y., Salman, T. M., Sánchez-Cano, B., Lynch, B. J., et al. (2024). On the mesoscale structure of coronal mass ejections at Mercury's Orbit: BepiColombo and Parker Solar Probe Observations. *The Astrophysical Journal*, *963*(2), 108. https://doi.org/10.3847/1538-4357/ad1ab4

Palmerio, E., Kay, C., Al-Haddad, N., Lynch, B. J., Trotta, D., Yu, W., et al. (2025). A coronal mass ejection encountered by four spacecraft within 1 AU from the Sun: Ensemble modelling of propagation and magnetic structure. *Monthly Notices of the Royal Astronomical Society*, *536*(1), 203–222. https://doi.org/10.1093/mnras/stae2606

Palmerio, E., Kilpua, E. K. J., Möstl, C., Bothmer, V., James, A. W., Green, L. M., et al. (2018). Coronal magnetic structure of earthbound CMEs and in situ comparison. *Space Weather*, *16*(5), 442–460. https://doi.org/10.1002/2017SW001767

Palmerio, E., Lee, C. O., Richardson, I. G., Nieves-Chinchilla, T., Dos Santos, L. F. G., Gruesbeck, J. R., et al. (2022). CME evolution in the structured heliosphere and effects at Earth and Mars during solar minimum. *Space Weather*, *20*(9), e2022SW003215. https://doi.org/10.1029/2022SW003215

Regnault, F., Al-Haddad, N., Lugaz, N., Farrugia, C. J., Yu, W., Zhuang, B., & Davies, E. E. (2024). Discrepancies in the properties of a coronal mass ejection on scales of 0.03 au as revealed by simultaneous measurements at solar orbiter and wind: The 2021 November 3–5 event. *The Astrophysical Journal*, *962*(2), 190. https://doi.org/10.3847/1538-4357/ad1883

Richardson, I. G., & Cane, H. V. (2010). Near-Earth interplanetary coronal mass ejections during solar cycle 23 (1996–2009): Catalog and summary of properties. *Solar Physics*, *264*(1), 189–237. https://doi.org/10.1007/s11207-010-9568-6

Richardson, I. G., & Cane, H. V. (2024). Near-Earth interplanetary coronal mass ejections since January 1996. *Harvard Dataverse*. https://doi.org/10.7910/DVN/C2MHTH

Riley, P., Linker, J. A., Lionello, R., Mikić, Z., Odstrcil, D., Hidalgo, M. A., et al. (2004). Fitting flux ropes to a global MHD solution: A comparison of techniques. *Journal of Atmospheric and Solar-Terrestrial Physics*, *66*(15–16), 1321–1331. https://doi.org/10.1016/j.jastp.2004.03.019

Rüdisser, H. T., Nguyen, G., Louëdec, J. L., Davies, E. E., & Möstl, C. (2025). Arcane—Early detection of interplanetary coronal mass ejections. Retrieved from https://arxiv.org/abs/2505.09365

Ruffenach, A., Lavraud, B., Farrugia, C. J., Démoulin, P., Dasso, S., Owens, M. J., et al. (2015). Statistical study of magnetic cloud erosion by magnetic reconnection. *Journal of Geophysical Research: Space Physics*, *120*(1), 43–60. https://doi.org/10.1002/2014JA020628

Salman, T. M., Lugaz, N., Farrugia, C. J., Winslow, R. M., Jian, L. K., & Galvin, A. B. (2020). Properties of the sheath regions of coronal mass ejections with or without shocks from STEREO in situ observations near 1 AU. *The Astrophysical Journal*, *904*(2), 177. https://doi.org/10.3847/1538-4357/abbdf5

Savani, N. P., Owens, M. J., Rouillard, A. P., Forsyth, R. J., Kusano, K., Shiota, D., & Kataoka, R. (2011). Evolution of coronal mass ejection morphology with increasing heliocentric distance. I. Geometrical analysis. *The Astrophysical Journal*, *731*(2), 109. https://doi.org/10.1088/0004-637X/731/2/109

Schwenn, R. (2006). Space weather: The solar perspective. *Living Reviews in Solar Physics*, *3*(1), 2. https://doi.org/10.12942/lrsp-2006-2

Scolini, C., Chané, E., Temmer, M., Kilpua, E. K. J., Dissauer, K., Veronig, A. M., et al. (2020). CME-CME interactions as sources of CME geoeffectiveness: The formation of the complex ejecta and intense geomagnetic storm in 2017 early September. *The Astrophysical Journal Supplement Series*, *247*(1), 21. https://doi.org/10.3847/1538-4365/ab6216

Smith, C. W., & Ness, N. F. (2022). *ACE magnetic field (MAG) geocentric solar ecliptic, GSE, and geocentric solar magnetospheric, GSM, coordinates, level 2 (H3), 1 s data*. Heliophysics Digital Resource Library (HDRL) dataset, 2022. HDRL. https://doi.org/10.48322/7XYH-4Z44

Sonnerup, B. U. O., & Cahill, L. J., Jr. (1967). Magnetopause structure and attitude from explorer 12 observations. *Journal of Geophysical Research*, *72*(1), 171. https://doi.org/10.1029/JZ072i001p00171

Stone, E. C., Frandsen, A. M., Mewaldt, R. A., Christian, E. R., Margolies, D., Ormes, J. F., & Snow, F. (1998). The advanced composition explorer. *Space Science Reviews*, *86*(1–4), 1–22. https://doi.org/10.1023/A:1005082526237

Thernisien, A., Vourlidas, A., & Howard, R. A. (2009). Forward modeling of coronal mass ejections using STEREO/SECCHI data. *Solar Physics*, *256*(1–2), 111–130. https://doi.org/10.1007/s11207-009-9346-5

Vourlidas, A., Wu, S. T., Wang, A. H., Subramanian, P., & Howard, R. A. (2003). Direct detection of a coronal mass ejection-associated shock in large angle and spectrometric coronagraph experiment white-light images. *The Astrophysical Journal*, *598*(2), 1392–1402. https://doi.org/10.1086/379098

Wang, Y., Shen, C., Wang, S., & Ye, P. (2004). Deflection of coronal mass ejection in the interplanetary medium. *Solar Physics*, *222*(2), 329–343. https://doi.org/10.1023/B:SOLA.0000043576.21942.aa

Webb, D. F., & Howard, T. A. (2012). Coronal mass ejections: Observations. *Living Reviews in Solar Physics*, *9*, 3. https://doi.org/10.12942/lrsp-2012-3

Wilson, L. B., III., Brosius, A. L., Gopalswamy, N., Nieves-Chinchilla, T., Szabo, A., Hurley, K., et al. (2021). A quarter century of wind spacecraft discoveries. *Reviews of Geophysics*, *59*(2), e2020RG000714. https://doi.org/10.1029/2020rg000714

Xystouris, G., Sigala, E., & Mavromichalaki, H. (2014). A complete catalogue of high-speed solar wind streams during solar cycle 23. *Solar Physics*, *289*(3), 995–1012. https://doi.org/10.1007/s11207-013-0355-z

Yu, W., Al-Haddad, N., Farrugia, C. J., Lugaz, N., Regnault, F., & Galvin, A. (2022). Investigating the asymmetry of magnetic field profiles of "Simple" magnetic ejecta through an expansion-modified flux rope model. *The Astrophysical Journal*, *937*(2), 86. https://doi.org/10.3847/1538-4357/ac88c3

Zurbuchen, T. H., & Richardson, I. G. (2006). In-situ solar wind and magnetic field signatures of interplanetary coronal mass ejections. *Space Science Reviews*, *123*(1–3), 31–43. https://doi.org/10.1007/s11214-006-9010-4